

Robust entangled photon generation enabled by single-shot Floquet driving

Jun-Yong Yan,^{1,*} Paul C. A. Hagen,^{2,*} Hans-Georg Babin,³ Wei E. I. Sha,¹ Andreas D. Wieck,³ Arne Ludwig,³ Chao-Yuan Jin,^{1,4} Vollrath M. Axt,² Da-Wei Wang,⁵ Moritz Cygorek,^{6,†} and Feng Liu^{1,4,‡}

¹State Key Laboratory of Extreme Photonics and Instrumentation,
College of Information Science and Electronic Engineering, Zhejiang University, Hangzhou 310027, China

²Theoretische Physik III, Universität Bayreuth, 95440 Bayreuth, Germany

³Lehrstuhl für Angewandte Festkörperphysik, Ruhr-Universität Bochum, Bochum, Germany

⁴International Joint Innovation Center, Zhejiang University, Haining 314400, China

⁵Zhejiang Key Laboratory of Micro-Nano Quantum Chips and Quantum Control,
School of Physics, Zhejiang University, Hangzhou 310027, China

⁶Condensed Matter Theory, Department of Physics, TU Dortmund, 44227 Dortmund, Germany

Quantum emitters driven by resonant two-photon excitation are a leading source for deterministically generated entangled photon pairs, essential for scalable photonic quantum technologies. However, conventional resonant schemes are highly sensitive to laser power fluctuations and pose additional experimental challenges for emitters with small biexciton binding energies. Here, we demonstrate how biexciton preparation schemes with significantly improved robustness and reduced laser filtering requirements can be identified using a novel design principle beyond resonant and adiabatic driving: *ultrafast single-shot Floquet driving*. This is achieved by employing two strongly and symmetrically detuned dichromatic pulses, whose superposition generates a stroboscopic Hamiltonian that enables direct coupling between ground and biexciton states. Moreover, a pulse delay serves as a tuning knob, introducing an effective magnetic field that concentrates the Bloch sphere trajectory at the biexciton state for a wide range of parameters, making biexciton preparation particularly robust. Experimentally, we achieve a biexciton occupation exceeding 96% and preserve photon-pair entanglement with a fidelity of 93.4%. Our scheme highlights the great impact of Floquet-engineered multicolour excitation protocols for on-demand quantum light sources.

Quantum entanglement, one of the most intriguing phenomena in the quantum world, lies at the heart of quantum information science. A deterministic source of entangled photons is a fundamental building block for modern quantum photonics applications, such as quantum communications [1, 2], optical quantum computing [3, 4], quantum imaging and sensing [5, 6]. A semiconductor quantum dot (QD), often referred to as an artificial atom due to its three-dimensional electronic confinement and discrete energy levels, is a well-established source of highly entangled photons [7–9]. The on-demand high-fidelity preparation of the biexciton state (BX) is the starting point for the radiative cascade decay process that generates entangled photon pairs. Moreover, cascade-emitted photons have been shown to induce simultaneous excitation of two independent quantum emitters [10], enabling the synthesis of effective multi-qubit interactions and coherent generation of entangled states [11].

A degenerate resonant two-photon excitation (TPE) scheme, where two photons with identical frequencies are absorbed simultaneously, is commonly used to coherently prepare the BX state with minimal dephasing and time jitter [12] (see Fig. 1(b)). This excitation scheme has shown significant potential in generating polarization-entangled photon pairs [13–15], time-bin entangled photons [16, 17] and indistinguishable single photons [18–20].

However, conventional TPE relies on Rabi oscillations of BX populations, making its excitation efficiency highly sensitive to variations in the excitation laser power and the dipole moment of the emitters. Furthermore, tuning the laser to the average frequency of the BX and X photons is unfavorable for QDs with small or negative BX binding energy (E_b). In the former case [21, 22], the tiny detuning between the laser and the entangled photon pairs makes it particularly difficult to perform effective laser filtering. In the latter case, the TPE process competes with phonon-assisted excitation of X , reducing the preparation efficiency of BX [23]. These limitations hinder the performance and scalability of on-demand entangled photon sources. Although several alternative approaches have been explored, including rapid adiabatic passage [24–26], LA-phonon-assisted excitation [27–29], and SUPER [30–32], simultaneous achievement of robust BX excitation and the generation of highly entangled photon pairs has yet to be demonstrated experimentally.

Floquet engineering, which employs periodic driving to achieve desired quantum dynamics, offers a fundamentally different route for overcoming the limitations of existing excitation schemes. According to Floquet’s theorem [33], when a quantum system is periodically driven with a period T , the time evolution operator evaluated at stroboscopic times (integer multiples of T) takes the same form as for a time-independent Hamiltonian (see Methods Section). This stroboscopic Hamiltonian governs the behaviour of the quantum system on a coarse-grained time scale $\gtrsim T$. Moreover, if the driving oscillates periodically within a slowly varying envelope, the

* These authors contributed equally to this work.

† Email to: moritz.cygorek@tu-dortmund.de

‡ Email to: feng-liu@zju.edu.cn

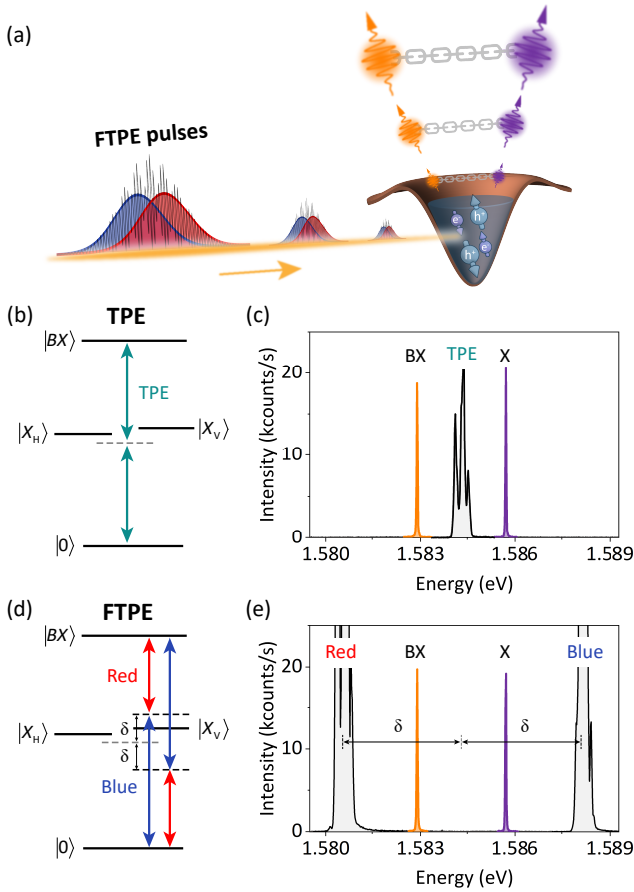


FIG. 1. **TPE and FTPE schemes.** **a**, Biexciton state prepared by FTPE emits pairs of entangled photons. **b**, Schematic of the TPE process. **c**, Laser excitation spectrum under TPE, where the energy of the TPE pulse is set at the average energy of the BX and X photons. **d**, Schematic of FTPE. **e**, Laser excitation spectrum under FTPE, where the blue and red pulse is detuned symmetrically to meet the two-photon resonance condition.

system approximately follows the instantaneous stroboscopic Hamiltonian, which is then time-dependent on the scale of the envelope [34]. The ability to control and tune the properties of quantum systems by Floquet engineering has enabled the realization of photonic topological insulators [35] and synthetic gauge fields in photonic [36] and in ultracold atomic systems [37].

Existing Floquet engineering approaches typically utilize modulated continuous-wave laser fields or repetitive laser pulse trains. In the context of on-demand semiconductor quantum light sources, Floquet engineering has focused mainly on engineering excitonic wave functions by periodic microwave driving [38]. Despite these advances, all-optical Floquet engineering with a *single-cycle pulses* to manipulate the optical excitation dynamics remains unexplored.

In this article, we propose and demonstrate a scheme for robust on-demand biexciton preparation and entan-

gled photon generation enabled by all-optical single-shot Floquet driving [Fig. 1(a)]. Our key observation is that one can realize a time-dependent stroboscopic Hamiltonian that directly drives the ground-to-biexciton transition of a semiconductor quantum dot simply by dichromatic excitation with laser pulses symmetrically detuned from the degenerated two-photon resonance by a detuning δ [Fig. 1(d) and (e)]. Further requirements are that the detuning is large enough so that oscillations with frequency δ are fast compared to changes in the pulse envelope and that the pulses overlap temporally. Control of the phase relation between the pulses is not required (see Supplementary Sect. V). These requirements are well achievable within current state-of-the-art experimental techniques for two-colour excitation [39–42]. Moreover, the dichromatic pulses can be detuned far from the X and BX photons, relaxing the requirement for laser filtering, especially for QDs with small or negative BX binding energy. Hence, our proposed excitation scheme, which we refer to as *Floquet-engineered Two-Photon Excitation* (FTPE) can be readily implemented to a wide range of QDs. In our experiments, we demonstrate a BX preparation efficiency of 96.1% and a polarization-entanglement fidelity of 93.4%, proving its reliability.

THEORY ON FLOQUET-ENGINEERED TWO-PHOTON EXCITATION

Figure 1(a) illustrates the proposed FTPE scheme applied to a semiconductor QD. A pair of temporarily partially overlapping dichromatic pulses (depicted in blue and red) generates a periodic driving field (indicated by gray lines). This periodic driving deterministically and reliably creates a biexciton in the QD, which subsequently emits entangled photon pairs via the cascade decay process.

To model the FTPE process, we consider a ladder system composed of a ground state $|0\rangle$, vertically (V) polarized exciton $|X_V\rangle$, and a biexciton state $|BX\rangle$. We assume that both driving lasers are vertically polarized such that the horizontally (H) polarized exciton is not involved in the excitation process. The energy of $|BX\rangle$ is $E_{BX} = 2E_X - E_b$, where E_X is the energy of the X state and E_b is the biexciton binding energy. Figure 1(b) shows the schematic of conventional TPE, where the laser is tuned to be strictly in resonance with the virtual state of the $|0\rangle$ to $|BX\rangle$ degenerate two-photon transition and Rabi oscillations can be observed [12]. A representative TPE laser excitation spectrum is presented in Fig. 1(c). The laser frequency is tuned to the midpoint between the BX and X emission lines. In contrast, as shown in Fig. 1(d), the two colour lasers used in FTPE are detuned to lie outside the BX and X lines. Thus, a large range of laser detunings is allowed as long as the two-photon resonance is maintained [43], i.e., $E_{\text{blue}} + E_{\text{red}} = E_{BX}$. The higher and lower energy lasers are labeled as blue and red pulses, respectively. Since the $|BX\rangle$ to $|X_V\rangle$ and $|X_V\rangle$

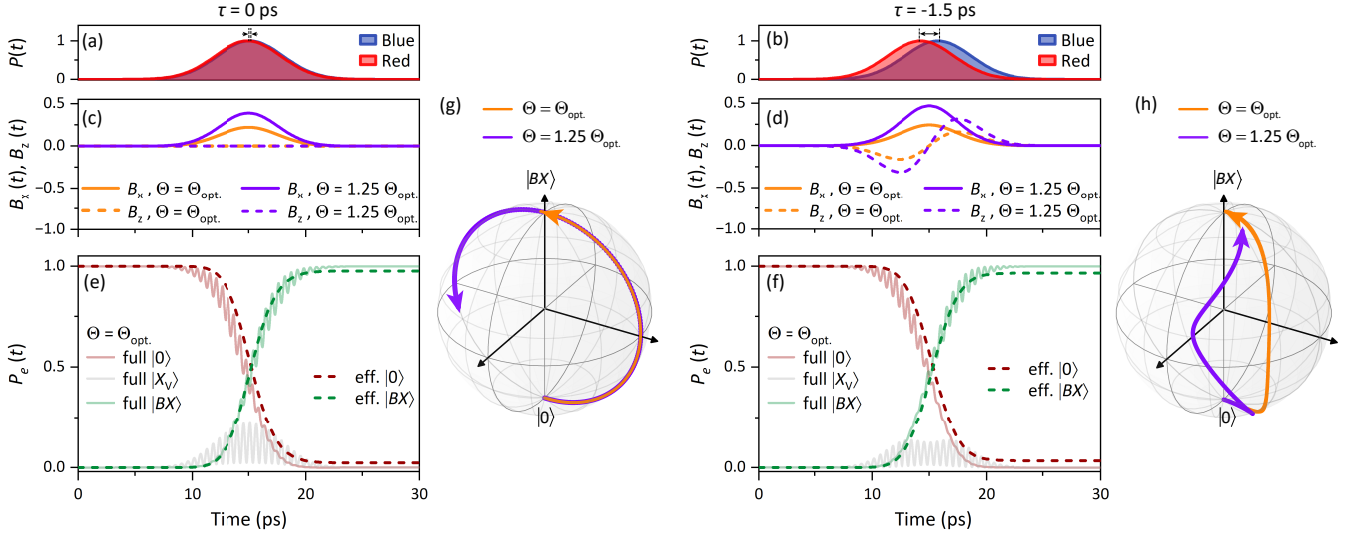


FIG. 2. **Simulated FTPE for different pulse delays τ .** **a** and **b**, time-dependent laser amplitudes of red and blue detuned pulses for delays $\tau = 0$ ps and $\tau = -1.5$ ps, respectively. **c** and **d**, time-dependence of the effective magnetic field components $B_x(t)$ and $B_z(t)$ in the stroboscopic two-level Hamiltonian in Eq. (2) for delays $\tau = 0$ ps and $\tau = -1.5$ ps and for their optimal driving strengths $\Theta = \Theta_{\text{opt.}} = 7.7\pi$ for $\tau = 0$ ps and $\Theta = \Theta_{\text{opt.}} = 8.3\pi$ as well as for driving strengths $\Theta = 1.25\Theta_{\text{opt.}}$, representing deviations from the optimal value. The detuning $\delta = 3.75$ meV was chosen. **e** and **f**, simulated time evolution of the QD state occupations for the respective optimal pulse areas for $\tau = -1.5$ ps, respectively. Full: solution from full Hamiltonian of Eq. (1). Eff.: solution from the effective stroboscopic model of Eq. (2). **g** and **h**, corresponding trajectories on the Bloch sphere of the effective two-level system composed of ground and biexciton states.

to $|0\rangle$ transitions have the same optical polarization selection rule, each laser pulse simultaneously couples to both transitions [Fig. 1(d)]. Figure 1(e) shows a representative laser excitation spectrum under FTPE. The detuning of either laser from conventional TPE resonance is labeled as δ . In the frame rotating with the frequency of resonant TPE ($E_{BX}/(2\hbar)$), the Hamiltonian in the basis $\{BX, X_V, 0\}$ is given by

$$H/\hbar = \begin{pmatrix} 0 & \Omega^*(t)/2 & 0 \\ \Omega(t)/2 & E_b/(2\hbar) & \Omega^*(t)/2 \\ 0 & \Omega(t)/2 & 0 \end{pmatrix}, \quad (1)$$

where the light-matter interaction term contains two equally strong laser pulses $\Omega(t) = f(t - \tau/2)e^{-i\delta t} + f(t + \tau/2)e^{i\delta t}$, which can be delayed relative to each other by a time τ . The individual pulse envelopes are Gaussian $f(t) = \frac{\Theta}{\sqrt{2\pi}s}e^{-t^2/2s^2}$ with pulse area Θ and Gaussian standard deviation $s = 4\sqrt{2\ln 2}\tau_0$ related to the pulse duration τ_0 . The full quantum dynamics of the driven QD including phonon effects [44, 45] is simulated using the numerically exact process tensor method [46, 47] (see Methods Section).

The working principle of our FTPE scheme can be understood by Floquet theory with respect to the period $T = 2\pi/\delta$. For detunings δ large enough so that $T \ll \tau_0$, fast oscillations can be eliminated and H is replaced by a stroboscopic Hamiltonian $H^{\text{eff.}}$, which is obtained by systematic expansion in $1/\delta$ [48, 49]. For our FTPE scheme, the second-order term is crucial because it enables direct transitions between the ground and biexciton states

(see Methods Section). Quantitatively relevant corrections are found up to the third order. For stroboscopic times, the exciton is hardly excited, which allows confining the Floquet analysis to the subspace composed predominantly of states $|BX\rangle$ and $|0\rangle$. We obtain the stroboscopic Hamiltonian

$$H^{\text{eff.}}(t) = \frac{\hbar}{2}(B_x(t)\sigma_x + B_z(t)\sigma_z), \quad (2)$$

where in analogy to spin-1/2 systems $B_x(t)$ and $B_z(t)$ correspond to time-dependent effective magnetic field components, which govern the precession of the state on the Bloch sphere. The effective fields are shaped by a combination of parameters of the exciting lasers, the biexciton binding energy and the detuning. In the special case of zero delay $\tau = 0$ between the pulses [Fig. 2(a) and (c)], we find $B_z(t) = 0$ and thus a Rabi-like dynamics with an effective pulse area $\int_{-\infty}^t B_x(t')dt'$ in the two-level system, which is a nonlinear function of the pulse area Θ of the original excitation pulses. Interestingly, to leading order, the effective pulse area scales as $\sim \Theta^2$ instead of the usual linear scaling (c.f. Eq. (9) in the Methods Section). For finite delay τ , $B_z(t)$ becomes nonzero [Fig. 2(b) and (d)], which facilitates the engineering of more complex dynamics.

The time evolution of ground, exciton, and biexciton occupations is shown in Fig. 2(e) and (f) for FTPE without and with time delay, respectively, for the optimal pulse area $\Theta_{\text{opt.}}$, which we define such that the first

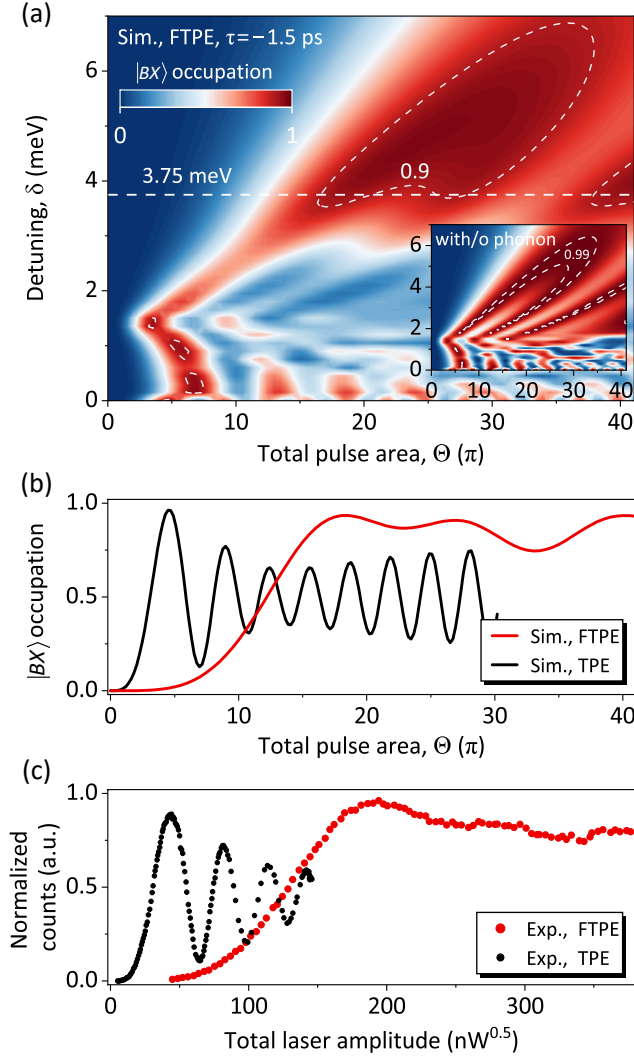


FIG. 3. **Deterministic and robust BX preparation via FTPE.** **a**, Calculated BX occupation versus total pulse area Θ and detuning δ with $\tau = -1.5$ ps. The horizontal line is where $\delta = 3.75$ meV as used in **b** and **c**. Inset: calculated values without phonon interaction. **b**, Theoretically calculated BX occupation as a function of total Θ , where exciton-phonon interaction and radiative decay are taken into account. **c**, Measured intensity of BX emission as a function of laser pulse amplitude, which is proportional to Θ , under TPE and FTPE. The counts are normalized with a scaling factor by fitting the TPE curve to simulations.

maximum in the final biexciton occupation is reached ($\Theta_{\text{opt.}} = 7.7\pi$ for $\tau = 0$ ps and $\Theta_{\text{opt.}} = 8.3\pi$ for $\tau = -1.5$ ps). The solid faded lines correspond to the solution of the full Hamiltonian Eq. (1), whereas the dashed lines describe the evolution according to the stroboscopic model of Eq. (2). Except for small-amplitude oscillations, the full numerical solution is well reproduced by the effective stroboscopic model. Thus, the behaviour of the physical system is indeed governed by the engineered effective magnetic field components $B_x(t)$ and $B_z(t)$. Fi-

nally, Fig. 2(g) and (h) show the respective behaviour on the Bloch sphere, of which the south pole corresponds to the ground state $|0\rangle$ and the north pole to the biexciton state $|BX\rangle$. To analyze the robustness of FTPE, we consider not only the optimal driving strengths $\Theta_{\text{opt.}}$ but also driving with increased pulse areas $1.25\Theta_{\text{opt.}}$ by scaling the envelopes $f(t)$ correspondingly. Without delay $\tau = 0$ (left panel) the Bloch sphere trajectories run along a great circle (due to $B_z = 0$). Thus, if the driving strength deviates from $\Theta_{\text{opt.}}$, the biexciton population decreases maximally, as the great circle describes the straightest line on the Bloch sphere. With finite delay $\tau = -1.5$ ps, the component $B_z(t)$ is found to be antisymmetric in time. This component twists the trajectories out of the yz -plane. Nevertheless, the biexciton state is reached for pulse area $\Theta_{\text{opt.}}$. Further increasing the driving strength not only increases the off-diagonal elements B_x of the stroboscopic model but also the effective detuning B_z . The enhanced twisting leads to an elongation of the trajectory from the ground to the biexciton state, such that overshooting, as found for $\tau = 0$ ps, is compensated. This mechanism is responsible for the significantly enhanced robustness found for certain delays τ .

EXPERIMENTS

To verify the experimental feasibility of the proposed FTPE scheme, we carry out the experiment with a single neutral droplet-etched GaAs/AlGaAs QD [50]. The sample is placed in a closed-cycle cryostat and cooled to 3.6 K. Transform-limited Gaussian pulses are generated from a femtosecond laser and stretched into two tunable 8.5-ps pulses using 4- f pulse shapers. The time delay τ between blue and red pulses is controlled by an optical delay line with a resolution of ~ 15 fs. The exciton fine-structure splitting (FSS) [51] due to the QD's natural anisotropy is effectively eliminated by a continuous-wave (CW) laser via the ac Stark effect [8]. As considered in the theoretical model, the polarizations of lasers are all aligned with the QD's V dipole orientation, thereby minimizing coupling with the H polarized exciton $|X_H\rangle$. More experimental details are provided in the Supplementary Section I.

ROBUST BIEXCITON PREPARATION USING FTPE

We first perform a two-dimensional simulation by scanning over the laser pulse area Θ and detuning δ to map the BX state preparation dynamics (Fig. 3a). This allows us to identify parameter regimes that enable efficient and robust BX state preparation. The results show that near-unity (98.7%) preparation efficiency is achievable despite the presence of phonons, and high efficiency ($> 90\%$) can be maintained across a wide range

of excitation conditions, demonstrating the robustness of the scheme. The theoretical model is described in the Methods Section, and it includes the full time-dependent Hamiltonian radiative decay as well as non-Markovian phonon effects, which are captured within the numerically exact process tensor framework ACE [46, 47]. The inset of Fig. 3(a) shows calculated results without phonon effects, confirming that phonon assistance is not essential for BX preparation. Without phonons, the reachable biexciton occupations are even higher, making the scheme even more attractive for emitters not affected by phonons, such as atomic systems.

Having identified the suitable laser pulse parameters, we next perform an experimental demonstration of FTPE. Fig. 3(c) shows experimentally measured BX emission (red dots) obtained under FTPE with $\delta = 3.75$ meV and optimal delay $\tau = -1.5$ ps. With increasing laser pulse area, the BX emission exhibits a gradual increase followed by a slightly fluctuating plateau. The pulse area dependence of the BX emission for other delays can be found in Supplementary Section II. As a comparison, the BX emission (black dots) obtained under conventional TPE shows the well-known Rabi oscillation. The main damping source of the Rabi oscillations comes from the QD-phonon coupling [52]. Both excitation schemes are well reproduced by our model [Fig. 3(b)]. As shown in Fig. 3(c), the first maximum of the BX occupation under TPE (black dots, 89%) occurs at a π pulse power of $1.95 \mu\text{W}$. The experimentally achieved occupations are calibrated by fitting the TPE Rabi oscillation data to numerical results with a normalization factor. The maximum BX occupation achieved under FTPE is $\sim 96\%$ and appears at $37.7 \mu\text{W}$. Importantly, the achieved final occupation shows significantly reduced sensitivity to variations in laser amplitude. This robustness to experimental fluctuations underscores the advantages of the FTPE scheme for practical quantum information applications.

ON-DEMAND GENERATION OF ENTANGLED PHOTONS

One promising application of our FTPE scheme is to deterministically generate entangled photon pairs. To assess the practicality, it is crucial to examine both the entanglement fidelity of the FTPE-generated photon pairs and the compatibility of the FTPE scheme with experimental techniques required for the collection and verification of entangled photons. To this end, we investigate the cascade emission from the BX state prepared by FTPE, which is operated as a source of polarization-entangled photon pairs [Fig. 4(a) inset]. Since the FTPE pulses are far detuned from BX and X photon emission peaks, they can be removed simply by spectral filters without affecting the polarization state of entangled photons. The entanglement fidelity is then characterized by separating BX and X photons using a polarization-insensitive

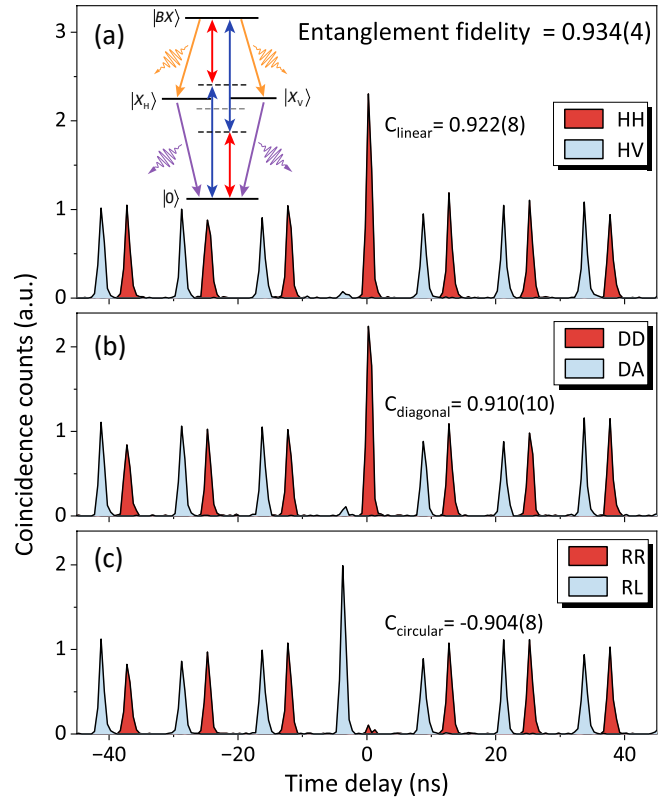


FIG. 4. Entanglement characterization under FTPE. **a**, Detected BX - X photon cross-correlation coincidence counts under FTPE in linear basis (H, horizontal; V, vertical). Inset: The cascade radiative recombination of BX state provides two polarization-entangled photons. **b**, In diagonal basis (D, diagonal; A, anti-diagonal). **c**, In circular basis (R, right circular; L, left circular).

grating, followed by the measurement of the polarization-dependent second-order correlation functions. The intrinsic FSS ($3.4(2) \mu\text{eV}$) is eliminated by the ac Stark effect induced with a $13.5 \mu\text{W}$ CW laser [8]. Figure 4 shows six cross-correlation measurements in the rectilinear [HH and HV, Fig. 4(b)], diagonal [DD and DA, Fig. 4(c)], and circular [RR and RL, Fig. 4(d)] polarization bases under FTPE, with each histogram composed of 500-ps time bins. By analyzing the degrees of polarization correlation (C_μ , where μ is the polarization basis), the fidelity to the Bell state $|\psi^+\rangle = \frac{1}{\sqrt{2}}(|H_{BX}\rangle|H_X\rangle + |V_{BX}\rangle|V_X\rangle)$ is obtained as:

$$f = \frac{1 + C_{\text{linear}} + C_{\text{diagonal}} - C_{\text{circular}}}{4} = 0.934(4). \quad (3)$$

The uncertainties are calculated using error propagation, assuming Poisson statistics for the coincidence counts. We note that the main limiting factor of the achieved f is re-excitation of the $|X_V\rangle \rightarrow |BX\rangle$ transition caused by the CW ac-Stark effect laser instead of the FTPE scheme itself. This is evidenced by the CW-power dependence of autocorrelation measurements (see Supplementary Section III). These results demonstrate that the FTPE pro-

TOCOL is a reliable method for generating highly entangled photon pairs.

DISCUSSION AND CONCLUSION

We have demonstrated the design and implementation of a robust biexciton state preparation scheme for a semiconductor quantum dot based on our concept of ultrafast all-optical Floquet engineering. Appropriately choosing the parameters of two differently coloured laser pulses lets us arrange a situation where the quantum dot experiences periodic driving within the laser duration. This allows us to engineer a stroboscopic Hamiltonian connecting the initial state with the target state of the protocol and to control the effective time-dependent driving between them. Thereby, we can identify a suitable parameter regime where FTPE is robust against fluctuations in the laser power and where detrimental phonon effects are also of minor importance. In particular, we have identified the delay between the two pulses to be a pivotal tuning knob for reaching the robust regime. The theoretical predictions are very well reproduced in our experiments.

The wide selectable laser detuning range of FTPE enhances experimental flexibility and relaxes the demand for laser filtering. Moreover, the high entanglement fi-

delity achieved suggests that the FTPE scheme does not induce additional dephasing channels, further validating its practicality for quantum information applications. Notably, the laser pulse parameters used in this work, such as duration, waveform, and chirp, can be further optimized. Future improvements could be realized through quantum optimal control [53], systematically tailoring these parameters to enhance the efficiency and robustness of state preparation.

As detailed in the Supplementary Section IV, the proposed FTPE scheme is distinct from other excitation schemes: the parameter regime for FTPE with detuning $\delta > E_B/(2\hbar)$ larger than half the biexciton binding energy is opposite to the limit of resonant TPE, which can be generalized to small but nonzero detuning $\delta \ll E_B/(2\hbar)$. Moreover, although robustness is also a feature found in adiabatic protocols, especially in the most robust region of finite pulse delays, FTPE is not adiabatic on an instantaneous eigenstate basis. The optical selection rules differ from STIRAP, and the resonance conditions of FTPE differ from those in other two-colour excitation schemes such as SUPER. These unique characteristics collectively highlight the distinctions of FTPE. Hence, the concept of all-optical single-shot Floquet driving establishes a foundation for developing a class of optimal excitation protocols tailored for quantum emitters, including molecules, atoms, colour centers, and superconducting qubits.

-
- [1] Zhang, W. *et al.* A device-independent quantum key distribution system for distant users. *Nature* **607**, 687–691 (2022).
 - [2] Li, Z.-D. *et al.* Experimental quantum repeater without quantum memory. *Nature Photonics* **13**, 644–648 (2019).
 - [3] Knill, E., Laflamme, R. & Milburn, G. J. A scheme for efficient quantum computation with linear optics. *Nature* **409**, 46–52 (2001).
 - [4] Kimble, H. J. The quantum internet. *Nature* **453**, 1023–1030 (2008).
 - [5] Defienne, H. *et al.* Advances in quantum imaging. *Nature Photonics* **18**, 1024–1036 (2024).
 - [6] Pirandola, S., Bardhan, B. R., Gehring, T., Weedbrook, C. & Lloyd, S. Advances in photonic quantum sensing. *Nature Photonics* **12**, 724–733 (2018).
 - [7] Huber, D. *et al.* Strain-Tunable GaAs Quantum Dot: A Nearly Dephasing-Free Source of Entangled Photon Pairs on Demand. *Physical Review Letters* **121**, 033902 (2018).
 - [8] Chen, C. *et al.* Wavelength-tunable high-fidelity entangled photon sources enabled by dual Stark effects. *Nature Communications* **15**, 5792 (2024).
 - [9] Chen, Y., Zopf, M., Keil, R., Ding, F. & Schmidt, O. G. Highly-efficient extraction of entangled photons from quantum dots using a broadband optical antenna. *Nature Communications* **9**, 2994 (2018).
 - [10] Muthukrishnan, A., Agarwal, G. S. & Scully, M. O. Inducing Disallowed Two-Atom Transitions with Temporally Entangled Photons. *Physical Review Letters* **93**, 093002 (2004).
 - [11] Ren, W. *et al.* Simultaneous Excitation of Two Noninteracting Atoms with Time-Frequency Correlated Photon Pairs in a Superconducting Circuit. *Physical Review Letters* **125**, 133601 (2020).
 - [12] Stuffer, S. *et al.* Two-photon Rabi oscillations in a single $\text{In}_x\text{Ga}_{1-x}\text{As}/\text{GaAs}$ quantum dot. *Physical Review B - Condensed Matter and Materials Physics* **73**, 1–7 (2006).
 - [13] Müller, M., Bounouar, S., Jöns, K. D., Glässl, M. & Michler, P. On-demand generation of indistinguishable polarization-entangled photon pairs. *Nature Photonics* **8**, 224–228 (2014).
 - [14] Liu, J. *et al.* A solid-state source of strongly entangled photon pairs with high brightness and indistinguishability. *Nature Nanotechnology* **14**, 586–593 (2019).
 - [15] Wang, H. *et al.* On-Demand Semiconductor Source of Entangled Photons Which Simultaneously Has High Fidelity, Efficiency, and Indistinguishability. *Physical Review Letters* **122**, 113602 (2019).
 - [16] Jayakumar, H. *et al.* Time-bin entangled photons from a quantum dot. *Nature Communications* **5**, 4251 (2014).
 - [17] Ginés, L. *et al.* Time-bin entangled photon pairs from quantum dots embedded in a self-aligned cavity. *Optics Express* **29**, 4174 (2021).
 - [18] Yan, J. *et al.* Double-Pulse Generation of Indistinguishable Single Photons with Optically Controlled Polarization. *Nano Letters* **22**, 1483–1490 (2022).
 - [19] Sbrenny, F. *et al.* Stimulated Generation of Indistinguishable Single Photons from a Quantum Ladder System. *Physical Review Letters* **128**, 093603 (2022).

- [20] Wei, Y. *et al.* Tailoring solid-state single-photon sources with stimulated emissions. *Nature Nanotechnology* **17**, 470–476 (2022).
- [21] Moroni, S. *et al.* Vanishing biexciton binding energy from stacked, MOVPE grown, site-controlled pyramidal quantum dots for twin photon generation. *Journal of Crystal Growth* **506**, 36–39 (2019).
- [22] Sarkar, D. *et al.* Exciton fine structure and biexciton binding energy in single self-assembled InAs/AlAs quantum dots. *Journal of Applied Physics* **100** (2006).
- [23] Juska, G. *et al.* Biexciton initialization by two-photon excitation in site-controlled quantum dots: The complexity of the antibinding state case. *Applied Physics Letters* **117**, 134001 (2020).
- [24] Glässl, M. *et al.* Biexciton state preparation in a quantum dot via adiabatic rapid passage: Comparison between two control protocols and impact of phonon-induced dephasing. *Phys. Rev. B* **87**, 085303 (2013).
- [25] Kaldewey, T. *et al.* Coherent and robust high-fidelity generation of a biexciton in a quantum dot by rapid adiabatic passage. *Physical Review B* **95**, 161302 (2017).
- [26] Karli, Y. *et al.* Robust single-photon generation for quantum information enabled by stimulated adiabatic rapid passage. *Applied Physics Letters* **125** (2024).
- [27] Quilter, J. H. *et al.* Phonon-Assisted Population Inversion of a Single InGaAs/GaAs Quantum Dot by Pulsed Laser Excitation. *Physical Review Letters* **114**, 137401 (2015).
- [28] Bounouar, S. *et al.* Phonon-assisted robust and deterministic two-photon biexciton preparation in a quantum dot. *Physical Review B* **91**, 161302 (2015).
- [29] Reindl, M. *et al.* Phonon-Assisted Two-Photon Interference from Remote Quantum Emitters. *Nano Letters* **17**, 4090–4095 (2017).
- [30] Bracht, T. K., Cygorek, M., Seidelmann, T., Axt, V. M. & Reiter, D. E. Temperature-independent almost perfect photon entanglement from quantum dots via the SUPER scheme. *Optica Quantum* **1**, 103 (2023).
- [31] Heinisch, N., Köcher, N., Bauch, D. & Schumacher, S. Swing-up dynamics in quantum emitter cavity systems: Near ideal single photons and entangled photon pairs. *Physical Review Research* **6**, L012017 (2024).
- [32] Kuniej, M., Gawelczyk, M. & Machnikowski, P. Hybrid acousto-optical swing-up preparation of exciton and biexciton states in a quantum dot (2024).
- [33] Shirley, J. H. Solution of the schrödinger equation with a hamiltonian periodic in time. *Phys. Rev.* **138**, B979–B987 (1965).
- [34] Ikeda, T. N., Tanaka, S. & Kayanuma, Y. Floquet-landau-zener interferometry: Usefulness of the floquet theory in pulse-laser-driven systems. *Phys. Rev. Res.* **4**, 033075 (2022).
- [35] Rechtsman, M. C. *et al.* Photonic Floquet topological insulators. *Nature* **496**, 196–200 (2013).
- [36] Cheng, D. *et al.* Non-Abelian lattice gauge fields in photonic synthetic frequency dimensions. *Nature* **637**, 52–56 (2025).
- [37] Weitenberg, C. & Simonet, J. Tailoring quantum gases by floquet engineering. *Nature Physics* **17**, 1342–1348 (2021).
- [38] Iorsh, I. V., Zezyulin, D. A., Kolodny, S. A., Sinitskiy, R. E. & Kibis, O. V. Floquet engineering of excitons in semiconductor quantum dots. *Phys. Rev. B* **105**, 165414 (2022).
- [39] Koong, Z. X. *et al.* Coherent dynamics in quantum emitters under dichromatic excitation. *Phys. Rev. Lett.* **126**, 047403 (2021).
- [40] Yan, J.-Y. *et al.* Coherent control of a high-orbital hole in a semiconductor quantum dot. *Nature Nanotechnology* **18**, 1139–1146 (2023).
- [41] Boyle, S., Ramsay, A., Fox, A. & Skolnick, M. Two-color two-photon Rabi oscillation of biexciton in single InAs/GaAs quantum dot. *Physica E: Low-dimensional Systems and Nanostructures* **42**, 2485–2488 (2010).
- [42] Yan, J.-Y. *et al.* All-Optical Ultrafast Arbitrary Rotation of Hole Orbital Qubits with Direct Phase Control. *Physical Review Letters* **133**, 203603 (2024).
- [43] Varada, G. V. & Agarwal, G. S. Two-photon resonance induced by the dipole-dipole interaction. *Physical Review A* **45**, 6721–6729 (1992).
- [44] Glässl, M., Barth, A. M. & Axt, V. M. Proposed Robust and High-Fidelity Preparation of Excitons and Biexcitons in Semiconductor Quantum Dots Making Active Use of Phonons. *Physical Review Letters* **110**, 147401 (2013).
- [45] Reiter, D. E., Kuhn, T., Glässl, M. & Axt, V. M. The role of phonons for exciton and biexciton generation in an optically driven quantum dot. *Journal of Physics: Condensed Matter* **26**, 423203 (2014).
- [46] Cygorek, M., Keeling, J., Lovett, B. W. & Gauger, E. M. Sublinear scaling in non-markovian open quantum systems simulations. *Phys. Rev. X* **14**, 011010 (2024).
- [47] Cygorek, M. & Gauger, E. M. Ace: A general-purpose non-markovian open quantum systems simulation toolkit based on process tensors. *The Journal of Chemical Physics* **161**, 074111 (2024).
- [48] Marin Bukov, L. D. & Polkovnikov, A. Universal high-frequency behavior of periodically driven systems: from dynamical stabilization to floquet engineering. *Advances in Physics* **64**, 139–226 (2015).
- [49] Takegoshi, K., Miyazawa, N., Sharma, K. & Madhu, P. K. Comparison among magnus/floquet/fer expansion schemes in solid-state nmr. *The Journal of Chemical Physics* **142**, 134201 (2015).
- [50] Kersting, E. *et al.* Shutter-Synchronized Molecular Beam Epitaxy for Wafer-Scale Homogeneous GaAs and Telecom Wavelength Quantum Emitter Growth. *Nanomaterials* **15**, 157 (2025).
- [51] Bayer, M. *et al.* Fine structure of neutral and charged excitons in self-assembled In(Ga)As/(Al)GaAs quantum dots. *Physical Review B* **65**, 195315 (2002).
- [52] Ramsay, A. J. *et al.* Damping of Exciton Rabi Rotations by Acoustic Phonons in Optically Excited InGaAs/GaAs Quantum Dots. *Physical Review Letters* **104**, 017402 (2010).
- [53] Werschnik, J. & Gross, E. K. U. Quantum optimal control theory. *Journal of Physics B: Atomic, Molecular and Optical Physics* **40**, R175–R211 (2007).

I. METHODS

A. Numerical methods

In our simulations, we include longitudinal acoustic (LA) phonons. Their coupling to the QD is included using the Hamiltonian

$$H_{\text{ph}}/\hbar = \sum_{\mathbf{q}} \omega_{\mathbf{q}} b_{\mathbf{q}}^{\dagger} b_{\mathbf{q}} + \sum_{\mathbf{q}, \nu} n_{\nu} (g_{\mathbf{q}} b_{\mathbf{q}} + g_{\mathbf{q}}^* b_{\mathbf{q}}^{\dagger}) |\nu\rangle\langle\nu|, \quad (4)$$

where $b_{\mathbf{q}}^{\dagger}$ ($b_{\mathbf{q}}$) is the creation (annihilation) operator for a LA phonon with wave vector \mathbf{q} and frequency $\omega_{\mathbf{q}}$, $|\nu\rangle \in \{|XV\rangle, |BX\rangle\}$ is the excitonic state and n_{ν} is the number of excitons present in the state $|\nu\rangle$. $g_{\mathbf{q}}$ denotes the coupling constant, which depends on crystal mass density, mode volume, material deformation potential and so on. We use these material parameters taken from the literature [1] and leave the electron (hole) wave function radius as the only free parameter, where the wavefunctions correspond to a harmonic confinement potential.

We solve the combined QD-phonon Hamiltonian using a state-of-the-art process tensor method [2–4]. This is necessary to accurately include phonons because it allows for short time-step length, which is necessary in this case due to the potentially large detunings δ . Other numerically complete methods, in particular, path-integral methods [5] would demand unfeasibly large amounts of memory.

B. Derivation of the effective Hamiltonian

Here, we summarize the mapping from the two-colour two-photon excitation of the three-level system composed of ground, exciton and biexciton states to an effective two-level system consisting predominantly of ground and biexciton states. We focus on the regime where the detuning δ is the dominant frequency scale. Then, the envelopes $f(t \pm \tau/2)$ in the driving term $\Omega(t) = f(t - \tau/2)e^{-i\delta t} + f(t + \tau/2)e^{i\delta t}$ vary slowly during a single oscillation period $T = 2\pi/\delta$.

To separate the time scales, we first assume the envelopes $f(t) \approx f$ to be constant over time T . We seek a stroboscopic Hamiltonian \bar{H} , which is similarly constant over short times $t \lesssim T$, but reproduces the time evolution over a single oscillation period T . It is defined by the condition

$$U(T) = e^{-\frac{i}{\hbar} \bar{H} T} \stackrel{!}{=} \mathcal{T} e^{-\frac{i}{\hbar} \int_0^T H(t) dt}, \quad (5)$$

where \mathcal{T} denotes the time-ordering operator. The stroboscopic Hamiltonian $\bar{H} = \bar{H}(f)$ parametrically depends on the pulse envelope f .

Thus, the dependence of \bar{H} on a coarse-grained time t can be reintroduced via the parametric dependence $\bar{H}(t) = \bar{H}(f(t))$.

While it is straightforward to obtain \bar{H} for a fixed value of f numerically, analytic insights can be gained by considering the Magnus expansion $\bar{H} = \sum_{n=0}^{\infty} \bar{H}^{(n)}$. The leading-order terms are given by [6]

$$\bar{H}^{(0)} = \frac{1}{T} \int_0^T dt_1 H(t_1) \quad (6a)$$

$$\bar{H}^{(1)} = \frac{-i}{2\hbar T} \int_0^T dt_1 \int_0^{t_1} dt_2 [H(t_1), H(t_2)], \quad (6b)$$

$$\begin{aligned} \bar{H}^{(2)} = & \frac{-1}{6\hbar^2 T} \int_0^T dt_1 \int_0^{t_1} dt_2 \int_0^{t_2} dt_3 \left([H(t_1), [H(t_2), H(t_3)]] \right. \\ & \left. + [H(t_3), [H(t_2), H(t_1)]] \right), \end{aligned} \quad (6c)$$

$$\begin{aligned} \bar{H}^{(3)} = & \frac{i}{12\hbar^3 T} \int_0^T dt_1 \int_0^{t_1} dt_2 \int_0^{t_2} dt_3 \int_0^{t_3} dt_4 \\ & \left([[H(t_1), H(t_2)], H(t_3)], H(t_4) \right] \\ & + [H(t_1), [[H(t_2), H(t_3)], H(t_4)]] \\ & + [H(t_1), [H(t_2), [H(t_3), H(t_4)]]] \\ & + [H(t_2), [H(t_3), [H(t_4), H(t_1)]]] \Big). \end{aligned} \quad (6d)$$

One finds that, to zeroth order, the dynamics on a coarse-grained timescale is governed by the time-averaged Hamiltonian $\bar{H}^{(0)}$. Yet the commutators in the higher-order terms can lead to qualitatively different transitions that are not directly visible from the original Hamiltonian $H(t)$.

For example, if there is no delay between the two pulses, $\Omega(t) = 2f(t) \cos(\delta t)$ and

$$\bar{H}^{(0)} = \begin{pmatrix} 0 & 0 & 0 \\ 0 & E_B/2 & 0 \\ 0 & 0 & 0 \end{pmatrix}, \quad (7a)$$

$$\bar{H}^{(1)} = 0, \quad (7b)$$

$$\bar{H}^{(2)} = \frac{E_B f}{4\hbar \delta^2} \left[\hbar f \begin{pmatrix} 1 & 0 & 1 \\ 0 & -2 & 0 \\ 1 & 0 & 1 \end{pmatrix} - E_B \begin{pmatrix} 0 & 1 & 0 \\ 1 & 0 & 1 \\ 0 & 1 & 0 \end{pmatrix} \right]. \quad (7c)$$

The zero-order term ensures that the exciton state remains off-resonant by energy $E_B/2$. Because n -th order terms scale as $1/\delta^n$ with the detuning δ , the zero-order term ensures that the excitonic state only becomes weakly occupied during the dynamics in the regime of interest where δ dominates. The first-order term vanishes when there is no delay between the pulses. Thus, the dynamics is mainly determined by

the second-order term $\bar{H}^{(2)}$, which itself consists of two contributions. The first provides corrections to the diagonal energies but more importantly drives direct transitions between the ground and the biexciton state with an effective Rabi frequency $E_B f^2(t)/(2\hbar\delta^2)$. The second contribution describes conventional transitions between ground and exciton and between exciton and biexciton states. However, as the exciton state is strongly off-resonant, the latter processes remain largely virtual and only lead to small quantitative corrections to the dynamics.

In fact, we find that the exciton state remains very weakly occupied even in the more complex case of finite delay between the pulses. This makes it possible to eliminate the exciton state altogether by a Schrieffer-Wolff transformation [7, 8]. There, the basis is slightly rotated by a unitary transformation such that coupling terms between the third, predominantly excitonic state and the remaining two states, which are predominantly composed of ground and biexciton state, vanish to leading order. To the second order, the effective two-level Hamiltonian is constructed from the stroboscopic Hamiltonian \bar{H} by

$$H_{m,n}^{\text{eff.}} = \bar{H}_{m,n} + \frac{1}{2} \left(\frac{\bar{H}_{m,XV} \bar{H}_{XV,n}}{\bar{H}_{m,m}^{(0)} - \bar{H}_{XV,XV}^{(0)}} + \frac{\bar{H}_{m,XV} \bar{H}_{XV,n}}{\bar{H}_{n,n}^{(0)} - \bar{H}_{XV,XV}^{(0)}} \right), \quad (8)$$

where $n, m \in \{BX, 0\}$. Higher-order Schrieffer-Wolff contributions are doubly suppressed, on the one hand by factors $1/\delta^n$ in the numerator, which stems from higher-order Magnus expansion terms (valid for $\delta \gg E_B$), and on the other hand by factors E_B^n in the Schrieffer-Wolff denominators (valid when E_B is much larger than the prefactors in $\bar{H}^{(m)}$ for $m > 0$). Doing this and introducing the time dependence of the laser envelopes, $f \rightarrow f(t)$, we obtain the effective Hamiltonian $H^{\text{eff.}} = \frac{\hbar}{2}(B_x(t)\sigma_x + B_z(t)\sigma_z)$ with components $B_x(t)$ and $B_z(t)$ obtained by comparison with Eq. (8).

For the case without delay, we can now also derive analytical formulas for the approximate biexciton occupation for different pulse amplitudes, using the well-known expressions from resonant Rabi systems. As was seen in Fig. 2 of this publications main body, the diagonal elements of (8) are zero for $\tau = 0$ ps, which gives an effective pulse area of

$$\Lambda := \int_{-\infty}^{\infty} H_{BX,0}^{\text{eff.}}(t) dt = \frac{E_B}{8\sqrt{\pi}\hbar\delta^2\sigma} \left(1 - \frac{E_B^2}{2\hbar^2\delta^2} \right) \Theta^2. \quad (9)$$

Using this, it is possible to calculate the final biexciton occupation using

$$|\langle BX | \psi(t = \infty) \rangle|^2 = \sin^2(\Lambda). \quad (10)$$

Importantly, the effective pulse area Λ scales with the square of the original pulse area Θ , which was used for

the two pulses.

DATA AVAILABILITY

The data that support this work are available from the corresponding author upon request.

CODE AVAILABILITY

The code that has been used for this work is available from the corresponding author upon request.

ACKNOWLEDGEMENT

We thank Dr. Doris Reiter for fruitful discussions. We acknowledge the Micro\Nano Fabrication Center at Zhejiang University for their facility support and technical assistance. F.L. acknowledges support from the National Key Research and Development Program of China (2022YFA1204700, 2023YFB2806000), the National Natural Science Foundation of China (62075194, U21A6006) and the National Supercomputer Center in Guangzhou. H.-G.B., A.D.W., and A.L. acknowledge support by the BMBF Project QR.N 16KIS2200, QuantERA BMBF EQSOTIC 16KIS2061, DFG ML4Q EXC 2004/1, and the DFH/UFA, Project CDFA-05-06. M.C. is supported by the Return Program of the State of North Rhine-Westphalia.

AUTHOR CONTRIBUTIONS

F.L. and M.C. conceived the project. H.-G.B., A.D.W. and A.L. grew the wafer and fabricated the sample. J.-Y.Y. built the setup and carried out the experiments. J.-Y.Y., P.C.A.H., M.C. and F.L. analysed the data. P.C.A.H. and M.C. performed the theoretical modeling. W.E.I.S., C.-Y.J., V.M.A., D.-W.W., M.C., and F.L. provided supervision and expertise. J.-Y.Y., P.C.A.H., M.C. and F.L. wrote the manuscript with comments and inputs from all the authors.

ADDITIONAL INFORMATION

Supplementary information is available in the online version of the paper. Correspondence and requests for materials should be addressed to Moritz Cygorek or Feng Liu.

COMPETING INTERESTS

The authors declare that they have no competing financial interests.

- [1] Krummheuer, B., Axt, V. M., Kuhn, T., D’Amico, I. & Rossi, F. Pure dephasing and phonon dynamics in gaas- and gan-based quantum dot structures: Interplay between material parameters and geometry. *Phys. Rev. B* **71**, 235329 (2005).
- [2] Jørgensen, M. R. & Pollock, F. A. Exploiting the causal tensor network structure of quantum processes to efficiently simulate non-markovian path integrals. *Phys. Rev. Lett.* **123**, 240602 (2019).
- [3] Cygorek, M. *et al.* Simulation of open quantum systems by automated compression of arbitrary environments. *Nature Physics* **18**, 662–668 (2022).
- [4] Cygorek, M. & Gauger, E. M. Ace: A general-purpose non-markovian open quantum systems simulation toolkit based on process tensors. *The Journal of Chemical Physics* **161**, 074111 (2024).
- [5] Vagov, A., Croitoru, M. D., Glässl, M., Axt, V. M. & Kuhn, T. Real-time path integrals for quantum dots: Quantum dissipative dynamics with superohmic environment coupling. *Physical Review B* **83**, 094303 (2011).
- [6] Takegoshi, K., Miyazawa, N., Sharma, K. & Madhu, P. K. Comparison among magnus/floquet/fer expansion schemes in solid-state nmr. *The Journal of Chemical Physics* **142**, 134201 (2015).
- [7] Schrieffer, J. R. & Wolff, P. A. Relation between the anderson and kondo hamiltonians. *Phys. Rev.* **149**, 491–492 (1966).
- [8] Winkler, R. *Spin-orbit Coupling Effects in Two-Dimensional Electron and Hole Systems* (Springer Berlin, Heidelberg, 2003).

Supplementary information: Robust entangled photon generation enabled by single-shot Floquet driving

Jun-Yong Yan*, Paul C. A. Hagen*, Hans-Georg Babin, Wei E. I. Sha, Andreas D. Wieck, Arne Ludwig, Chao-Yuan Jin, Vollrath Martin Axt, Da-Wei Wang, Moritz Cygorek[†], and Feng Liu[‡]

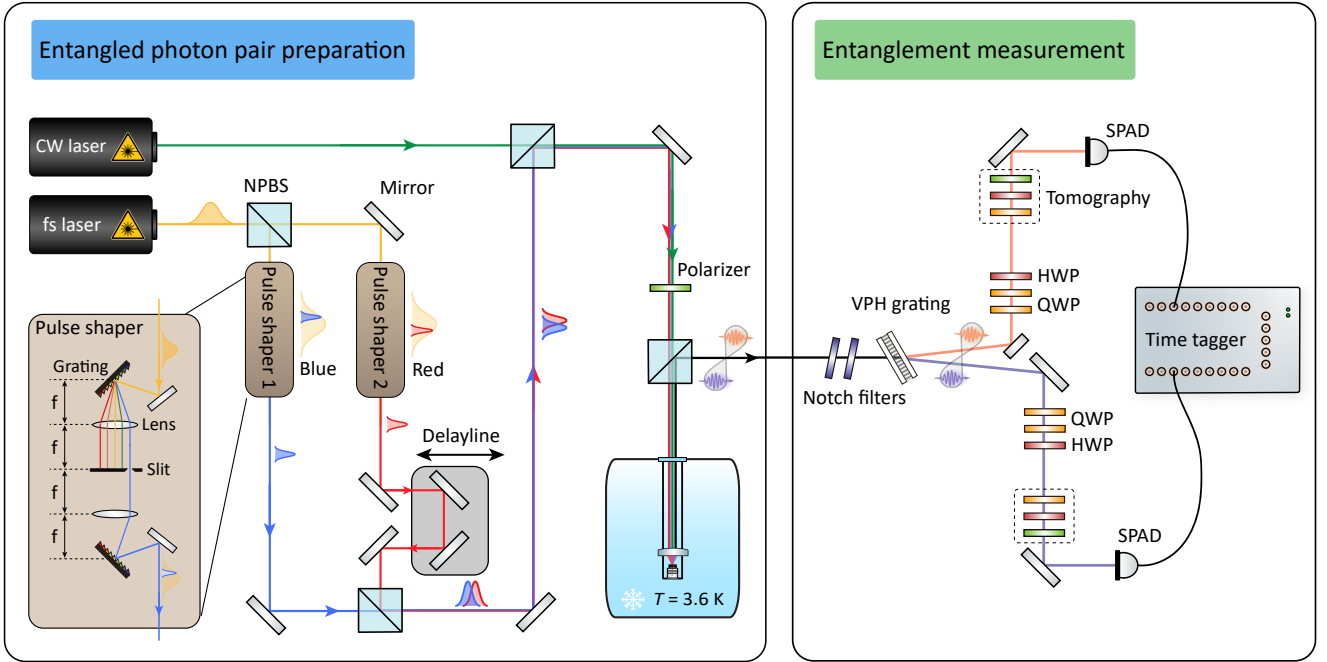
CONTENTS

I. Experimental setup	2
II. Biexciton preparation efficiency at different pulse delays	2
III. Tuning QD FSS via ac Stark effect	3
IV. Comparison with other excitation mechanisms	4
A. Nearly monochromatic two-photon resonant excitation	4
B. Adiabatic protocols	4
C. STIRAP	6
D. Other two-colour excitation schemes	6
V. Relative phase difference between the lasers	7
References	7

I. EXPERIMENTAL SETUP

A schematic of the optical characterization setup is illustrated in SFig. 1. The QD sample is placed in the 3.6-K cryostat (attocube, attoDRY1000). Transform-limited femtosecond pulses are generated by a Ti-sapphire oscillator (Coherent, Chameleon Ultra II) and subsequently split and shaped into a pair of ~ 8 ps pulses with different colours (denoted blue and red) by two pulse shapers. The temporal delay between the blue and red pulses is controlled by an optical delay line (Newport, DL235). A tunable CW laser (M squared, SolsTiS) is tuned to slightly red-detuning respect to the $|BX\rangle \rightarrow |XV\rangle$ transition and used to tune the QD FSS. The polarization of both the pulsed and CW lasers is aligned with the V dipole orientation of the QD, ensuring minimal coupling to the H dipole.

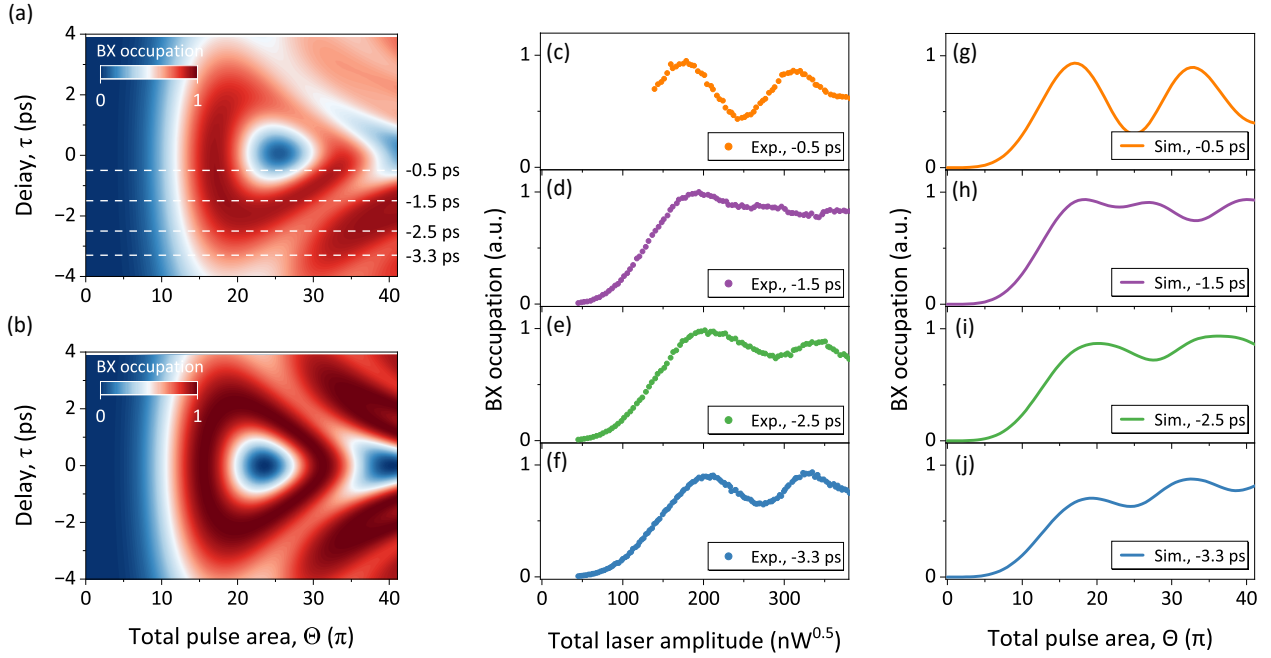
The emitted photons are collected by an aspheric objective lens (Thorlabs, NA = 0.7) and directed to a custom-built entanglement measurement setup. A filtering system, comprising a volume phase holographic transmission grating (Coherent, T-1400-800) and notch filters (Optigrade, BragGrate), is employed to spectrally eliminate laser scattering and separate the BX and X photons. A set of wave plates (Thorlabs), including two QWPs and one HWP, is used to compensate for polarization misalignment between the QD emission and the tomography basis [S1, S2]. Finally, the entangled photons are projected onto different polarization bases and then detected by two single-photon avalanche detectors (Excelitas, SPCM-AQRH) for cross-correlation measurements.



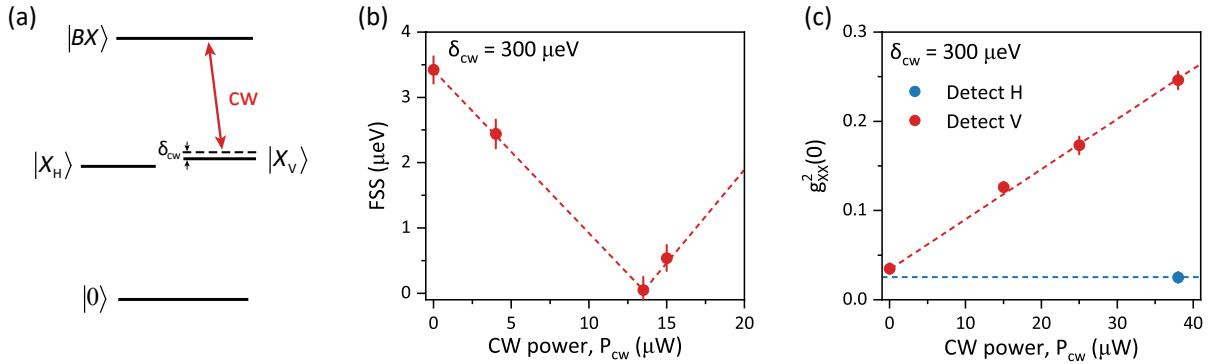
Supplementary Figure 1. **Sketch of the experimental setup.** The setup consists of two main parts: entangled photon pair preparation and entanglement measurements. NPBS: non-polarizing beam splitter; VPH grating: volume phase holographic grating; HWP: half-wave plate; QWP: quarter-wave plate; SPAD: single-photon avalanche diode.

II. BIEXCITON PREPARATION EFFICIENCY AT DIFFERENT PULSE DELAYS

To determine the optimal pulse delay, we simulated the BX occupation's dependence on pulse area at different pulse delays, both with (SFig.2(a)) and without (SFig.2(b)) considering QD-phonon coupling. As shown in SFig. 2(c-f), we measured the laser pulse dependence curves at $\tau = -0.5, -1.5, -2.5$, and -3.3 ps, from which an optimal operation delay of $\tau = -1.5$ ps was deduced. SFig.2(g-j) shows the corresponding simulation curves, which agree well with the experimental observations.



Supplementary Figure 2. **Pulse area dependence of BX occupation at different pulse delay.** **a**, Calculated BX occupation versus Θ and τ with $\hbar\delta = 3.75$ meV. **b**, Calculated values without phonon interaction. **c-g**, Measured BX occupations as a function of total laser amplitude for $\tau = -0.5, -1.5, -2.5$, and -3.3 ps. **h-l**, Calculated BX occupations as a comparison with experimental results.



Supplementary Figure 3. **FSS erasure via ac Stark effect.** **a**, ac Stark effect and QD energy level diagram. **b**, FSS as a function of applied CW laser power. Error bars arise from the standard error of sine fit residuals. **c**, Polarization-resolved autocorrelation measurements of $|BX\rangle \rightarrow |XV\rangle$ photons.

III. TUNING QD FSS VIA AC STARK EFFECT

To eliminate the FSS of the QD, we apply a vertical linear polarized CW laser slightly detuned from the $|BX\rangle \leftrightarrow |X_V\rangle$ transition (SFig. 3a). This allows us to tune the FSS by varying the power of the CW laser according to:

$$\Delta_{\text{FSS}} = \frac{1}{2} \left(\delta_{\text{CW}} - \sqrt{\delta_{\text{CW}}^2 + \Omega^2} \right). \quad (\text{S1})$$

The QD investigated in the main text is QD A. Supplementary Fig. 3(b) presents the experimentally measured FSS as a function of CW laser power. An optimal operating power of $13.5 \mu\text{W}$ is identified, where the FSS is almost eliminated. However, we observe a reduction in the single-photon purity of the $|BX\rangle \rightarrow |X_V\rangle$ photon pair with increasing CW power (Supplementary Fig. 3(c)). We attribute this effect to re-excitation of the $|X_V\rangle \leftrightarrow |BX\rangle$

transition by the CW laser following the $|BX\rangle \rightarrow |X_V\rangle$ emission, which can lead to twice $|BX\rangle$ emissions within a single excitation cycle. Since the CW laser exclusively couples to the V-polarized transition, the single-photon purity of the $|BX\rangle \rightarrow |X_H\rangle$ photon remains unaffected. This limit can be overcome by further increasing the CW-laser detuning or selecting QDs with a smaller intrinsic FSS.

IV. COMPARISON WITH OTHER EXCITATION MECHANISMS

A. Nearly monochromatic two-photon resonant excitation

While conventional monochromatic two-photon excitation is described by the same Hamiltonian as in Eq. (1) in the limit of zero detuning $\delta \rightarrow 0$, it is important to note that FTPE and TPE are qualitatively different and appear in opposite parameter regimes with no smooth transition in between them. It is instructive to consider the prediction of the usual description of TPE [S3] when a finite detuning δ is accounted for. Here, we focus on the case of zero delay $\tau = 0$ between the pulses, where the driving is given by

$$\Omega(t) = 2f(t) \cos(\delta t). \quad (\text{S2})$$

In contrast to the description of FTPE valid for large detunings, TPE is described using an adiabatic approximation [S3]. There the initial state $|G\rangle$ is decomposed into laser-dressed eigenstates. Over the pulse duration, the occupation of the instantaneous eigenstates is assumed to be constant by the adiabatic theorem, while the respective components of the wave function acquire dynamical phases corresponding to the time integral over the respective energy eigenvalues. The final biexciton state occupation $|\langle BX|\Psi\rangle|^2$ is then the result of the interference of the different eigenstate components of the wave function. One finds [S3]

$$|\langle BX|\psi\rangle|^2 = \sin^2 \frac{\Lambda}{2}, \quad (\text{S3})$$

with

$$\Lambda = \frac{1}{4\hbar} \int_{-\infty}^{\infty} \left[E_B - \sqrt{E_B^2 + 4 \cdot 8\hbar^2 \Omega^2(t)} \right] dt. \quad (\text{S4})$$

The final biexciton state occupations are depicted in Fig. 4 for both direct numerical simulations of the dynamics and the results of the adiabatic approximation. Indeed, for small detunings $\delta \ll E_B/(2\hbar)$, the adiabatic approximation captures the Rabi-like behaviour of the full dynamics well. However, for larger detunings, here $\delta \gtrsim E_B/(4\hbar)$, the adiabatic approximation starts to break down and the distribution of parameter sets for which a significant biexciton population is achieved becomes erratic.

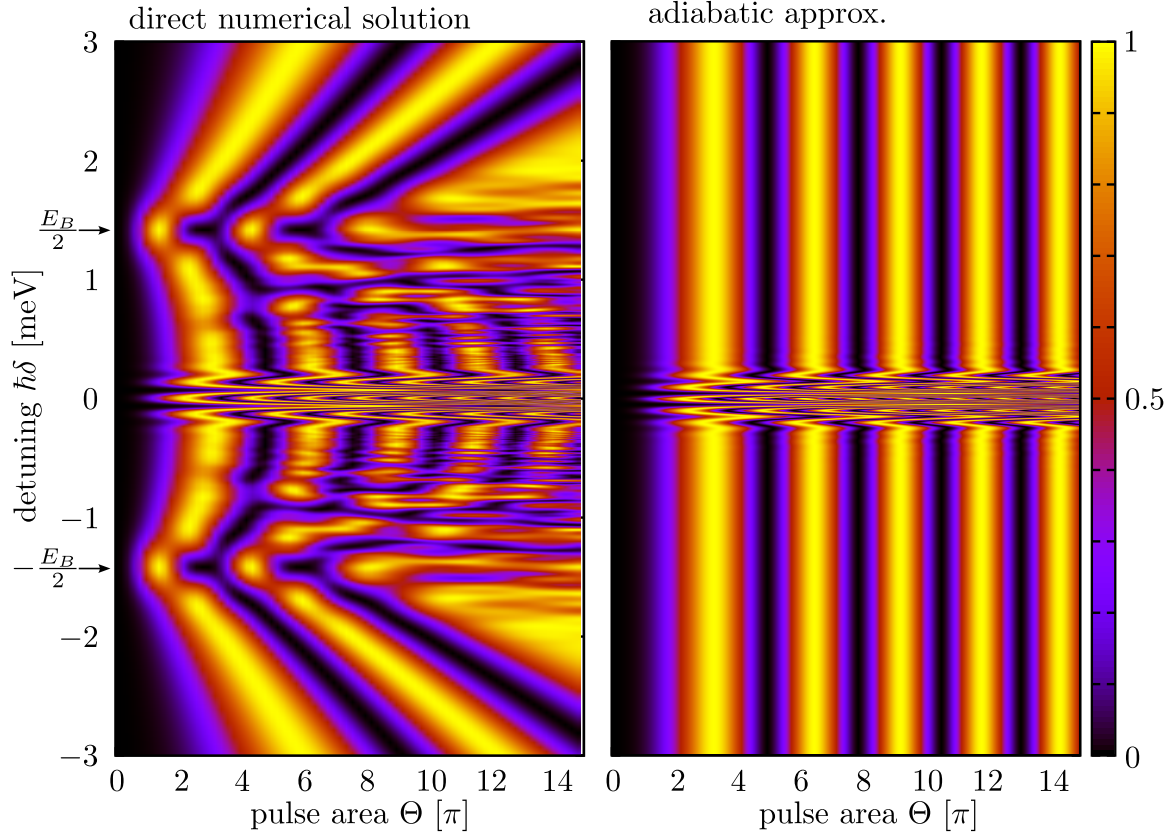
Clearly, at $\delta = E_B/(2\hbar)$ the lasers are resonant to direct transitions involving the single exciton state. Thus, even though near TPE and FTPE have in common that they involve virtual transitions without significant occupation of the exciton state, they are clearly distinguished by the parameter regimes $\delta < E_B/(2\hbar)$ and $\delta > E_B/(2\hbar)$. Thus, the physics in both regimes is different, which is why a different theoretical approach is required to explain FTPE.

The approximation only fits well for small detunings $\delta \ll E_B/2\hbar$

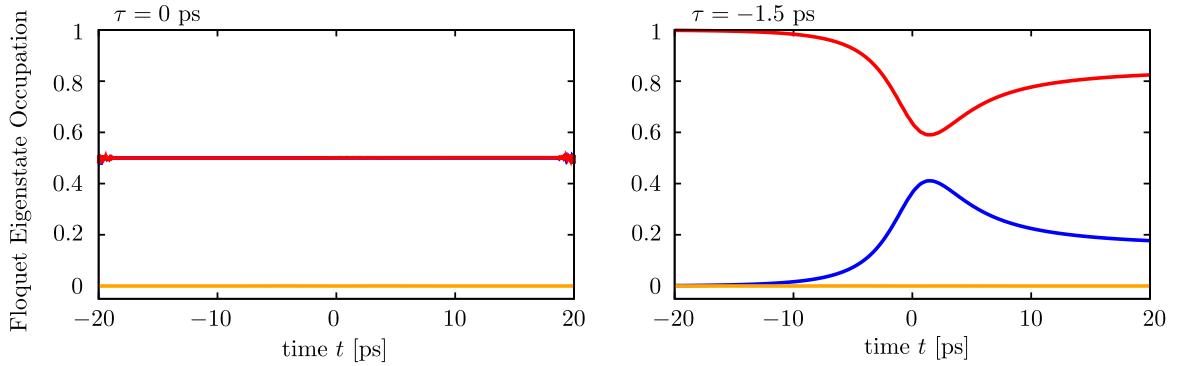
B. Adiabatic protocols

A number of state preparation protocols for quantum dots have been proposed that rely on adiabatic driving, such as adiabatic rapid passage using a chirped laser pulse [S4], whose frequency changes over time, or ultrafast electric tuning [S5]. Also phonon-assisted state preparation employs adiabatic undressing [S6] as a working principle. In particular, adiabatic protocols with the state of the systems confined to the lowest instantaneous eigenstate for most of the evolution are robust against small variations, e.g., of the pulse area. This raises the question of whether the robustness found for FTPE is related to adiabatic transitions.

To this end, we depict in Fig. 5 the occupations of instantaneous eigenstates of the stroboscopic Hamiltonian for parameters $\hbar\delta = 3.75$ meV and $E_B/2 = 1.41$ meV for cases without ($\tau = 0$ ps) and with ($\tau = -1.5$ ps) a delay between the pulses for FTPE. For finite delay, it can be seen that the dynamics is clearly nonadiabatic in the instantaneous eigenbasis of the stroboscopic Hamiltonian. Nevertheless, the dynamics is found to be robust. For vanishing delay, the occupations of instantaneous eigenstates remain nearly constant, similar to the behaviour



Supplementary Figure 4. Numerically calculated final biexciton population under near-two-photon resonant excitation as a function of detuning δ and pulse area per pulse Θ obtained by (a) direct numerical simulation of the three-level dynamics and (b) using the adiabatic approximation Eq. (S3). Half the biexciton binding energy is chosen as $E_B/2 = 1.41$ meV and quantum dot-phonon interactions are neglected in both calculations.



Supplementary Figure 5. Time evolution of the occupation of all three eigenstates of the stroboscopic Hamiltonian \bar{H} . Displayed are cases without any delay, $\tau = 0$ ps, as well as a small negative delay, $\tau = -1.5$ ps. Adiabatic transitions require occupations of instantaneous eigenstates to be constant in time, which is not fulfilled for finite detunings.

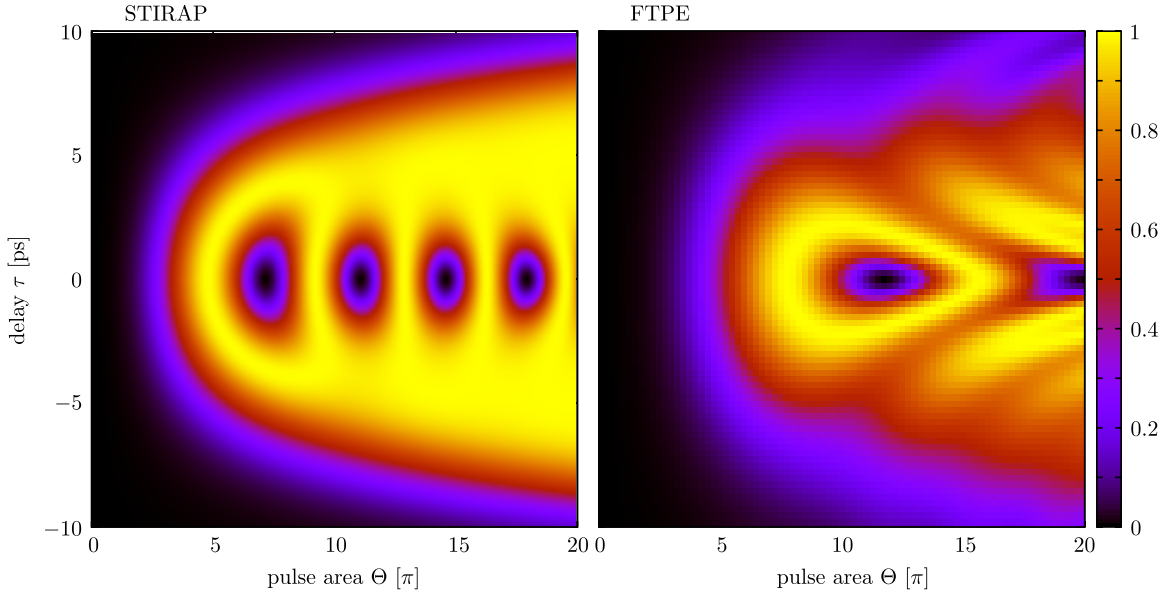
expected in the adiabatic limit. But because the system is in a coherent superposition between two eigenstates, the relative phase is generally sensitive to variations in the pulse area, making the protocol not more robust than, e.g., Rabi driving. To summarize, in the Floquet regime, the dynamics may or may not be adiabatic, dependent on the pulse delay, and the enhanced robustness is mainly found in the diabatic regime. This shows that the physics of FTPE differs from that of conventional adiabatic protocols.

C. STIRAP

A state preparation scheme whose setup, on first glance, resembles FTPE is stimulated Raman adiabatic passage (STIRAP) [S7]. STIRAP is designed to drive transitions between two ground states via a third, intermediate states. One assumes selection rules where the first (pump) pulse couples only the first ground state to the intermediate state and the second (stokes) pulse couples the intermediate state to the second ground state. Furthermore, both lasers are detuned from the respective transition with the same detuning Δ . In the basis of second ground, intermediate, and first ground state, the corresponding Hamiltonian is given by

$$H^{\text{STIRAP}} = \hbar \begin{pmatrix} 0 & \frac{\Omega_p}{2} & 0 \\ \frac{\Omega_p}{2} & \Delta & \frac{\Omega_s}{2} \\ 0 & \frac{\Omega_s}{2} & 0 \end{pmatrix}. \quad (\text{S5})$$

where $\Omega_p(t)$ and $\Omega_s(t)$ are the (real) amplitudes of the pump and Stokes pulse, respectively. The Hamiltonian is similar to Eq. (1) when the detunings are identified by $\Delta = \delta - E_B/(2\hbar)$. The delay and pulse area dependence of both STIRAP and FTPE for these parameters are depicted in Fig. 6. Both show Rabi rotations for zero delay and broad parameter regimes with large final state occupations.



Supplementary Figure 6. Comparison of the τ - Θ dependence of the biexciton occupation for regular STIRAP and FTPE. Θ is the pulse area of either individual laser. The detuning to the central level was chosen $\hbar\Delta = 2.34$ meV in both cases. The calculations were done without phonons.

However, there are also clear differences between STIRAP and FTPE. Most importantly, for STIRAP, the transitions can be controlled separately by the two laser pulses. The optical selection rules in the biexciton-exciton system of a quantum dot, on the other hand, are such that linearly polarized lasers couple both transitions simultaneously by both pulses. Even in the case of two lasers with oppositely circularly polarized pulses, for which the first pulse couples the ground state to an intermediate exciton state in the circular polarization basis and the second pulse couples the same exciton state to the biexciton state, the situation deviates from STIRAP, since for finite overlap of the pulses transitions to the exciton state with opposite polarization (a fourth level) are possible. Either way, the optical selection rules for semiconductor quantum dots prohibit the straightforward implementation of STIRAP for biexciton state preparation.

D. Other two-colour excitation schemes

Recently, two-colour excitation schemes have been explored for state preparation of quantum dots, in particular, exciton state preparation for applications in on-demand single-photon generation [S8, S9]. An important goal of

off-resonant excitation is that photons from the excitation laser can be easily spectrally separated from the emitted quantum state of light. A detailed analysis of the Swing-UP of quantum Emitter Population (SUPER) scheme has revealed that parameters for which off-resonant two-colour excitation leads to near-unity population inversion are found when one laser becomes resonant with the transition between the laser-dressed states Stark-shifted by the other laser [S10]. It was also predicted that the principle of the SUPER scheme can be used to efficiently populate the biexciton state using two-colour off-resonant excitation [S11].

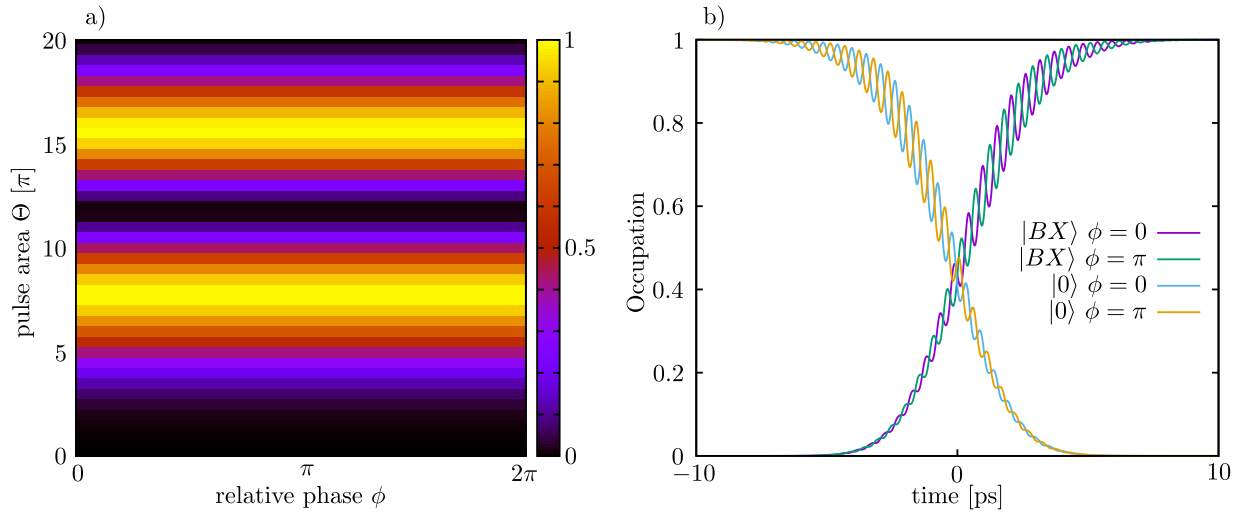
FTPE has in common with SUPER mainly the fact that two-colour off-resonant excitation is employed. But in contrast to SUPER, the Stark shift plays no role for FTPE and the resonance conditions differ.

V. RELATIVE PHASE DIFFERENCE BETWEEN THE LASERS

It is possible to add a relative phase ϕ to one of the lasers. Then, the laser function reads

$$\Omega(t) = f(t - \tau/2)e^{-i\delta t} + f(t + \tau/2)e^{i(\delta t + \phi)}. \quad (\text{S6})$$

The numerical investigations in Fig. 7(a) show that the relative phase between the lasers is irrelevant for the final occupation. Our protocol produces the same excitation regardless of the specific value of ϕ . It is similar to SUPER in this aspect. But, again like for SUPER, the oscillations during the excitation are affected, as can be seen in Fig. 7(b).



Supplementary Figure 7. **a)** Biexciton occupation after using two pulses with pulse area Θ in which one has the relative phase ϕ , as in Eq. (S6). $\hbar\delta = 3.75$ meV was chosen as a typical value and no delay between the lasers was used. The occupation clearly does not depend on the relative phase between the pulses. We find that the same applies in cases of $\tau \neq 0$ (not shown). **b)** The occupation of ground and biexciton states for two exemplary phases $\phi \in \{0, \pi\}$.

-
- [S1] Zhou, L. *et al.* Polarization Calibration Scheme for a Practical Handheld Free Space Quantum Key Distribution Link. In *2019 IEEE Globecom Workshops (GC Wkshps)*, 1–5 (IEEE, 2019).
 - [S2] Shao-Kai, W., Ji-Gang, R., Cheng-Zhi, P., Shuo, J. & Xiang-Bin, W. Realization of Arbitrary Inverse Unitary Transformation of Single Mode Fibre by Using Three Wave Plates. *Chinese Physics Letters* **24**, 2471–2474 (2007).
 - [S3] Stuffer, S. *et al.* Two-photon Rabi oscillations in a single $\text{In}_x\text{Ga}_{1-x}\text{As}/\text{GaAs}$ quantum dot. *Physical Review B - Condensed Matter and Materials Physics* **73**, 1–7 (2006).
 - [S4] Gawarecki, K. *et al.* Adiabatic rapid passage in quantum dots: phonon-assisted decoherence and biexciton generation. *physica status solidi c* **10**, 1210–1213 (2013).
 - [S5] Mukherjee, A. *et al.* Electrically controlled rapid adiabatic passage in a single quantum dot. *Applied Physics Letters* **116** (2020).
 - [S6] Barth, A. M. *et al.* Fast and selective phonon-assisted state preparation of a quantum dot by adiabatic undressing. *Phys. Rev. B* **94**, 045306 (2016).
 - [S7] Bergmann, K., Vitanov, N. V. & Shore, B. W. Perspective: Stimulated Raman adiabatic passage: The status after 25 years. *The Journal of Chemical Physics* **142**, 170901 (2015).

- [S8] He, Y.-M. *et al.* Coherently driving a single quantum two-level system with dichromatic laser pulses. *Nature Physics* **15**, 941–946 (2019).
- [S9] Koong, Z. X. *et al.* Coherent dynamics in quantum emitters under dichromatic excitation. *Phys. Rev. Lett.* **126**, 047403 (2021).
- [S10] Bracht, T. K. *et al.* Swing-up of quantum emitter population using detuned pulses. *PRX Quantum* **2**, 040354 (2021).
- [S11] Bracht, T. K., Cygorek, M., Seidelmann, T., Axt, V. M. & Reiter, D. E. Temperature-independent almost perfect photon entanglement from quantum dots via the SUPER scheme. *Optica Quantum* **1**, 103 (2023).